Rapid Communications

Additional excitonic features and momentum-dark states in ReS_2

A. Dhara, D. Chakrabarty, P. Das, A. K. Pattanayak, S. Paul, S. Mukherjee, and S. Dhara*
Department of Physics, IIT Kharagpur, Kharagpur WB 721302, India

(Received 31 July 2020; revised 30 September 2020; accepted 30 September 2020; published 16 October 2020)

Unidirectional in-plane structural anisotropy in rhenium-based dichalcogenides introduces a new class of 2D materials, exhibiting anisotropic optical properties. In this work, we perform temperature-dependent, polarization-resolved photoluminescence and reflectance measurements on several-layer ReS_2. We discover two additional excitonic resonances (X_3 and X_4), which can be attributed to the splitting of spin degenerate states. Strong in-plane oscillator strength of exciton species X_1 and X_2 is accompanied by weaker counterparts X_3 and X_4 with similar polarization orientations. The in-plane anisotropic dielectric function has been obtained for ReS_2, which is essential for engineering light matter coupling for polarization-sensitive optoelectronic devices. Furthermore, our temperature-dependent study revealed the existence of low-lying momentum-forbidden dark states causing an anomalous PL intensity variation at 30 K, which has been elucidated using a rate equation model involving phonon scattering from these states. Our findings of the additional excitonic features and the momentum-dark states can shed light on the true nature of the electronic band structure of ReS_2.

DOI: 10.1103/PhysRevB.102.161404

Introduction. In-plane structural anisotropy in individual layers of van der Waals materials produces electronic band structures that are unique in contrast to the family of transition metal dichalcogenides (TMDCs) with in-plane rotational symmetry. Rhenium (Re) based group VII TMDCs like ReS_2 have garnered considerable attention because of their intriguing anisotropic optical, vibrational, and electronic properties arising from reduced crystal symmetry [1–14]. This originates from ReS_2s distorted 1T structure [15], where the extra electron from the Re atom contributes to the strong Re-Re metal bond, forming a zigzag chain along the *b* axis. This results in higher electron mobility along the *b* axis [9] and optical anisotropy manifesting itself as highly polarized photoluminescence (PL) and absorption due to two strongly bound exciton species X_1 and X_2 with dipole moments along different in-plane directions [1,5–7]. These properties open the door to a class of polarization-sensitive, on-chip devices like polarization-controlled all-optical switches [16], polarized LEDs [17], photodetectors [18], and polarization-based quantum logic gates [19]. Additionally, for group VI TMDCs, the electronic and optical properties are strongly dependent on the number of layers of the crystal, and show a drastic change in the monolayer limit [20]. Conversely, ReS_2 with its weak interlayer coupling shows no such drastic change when going from bulk to monolayer [2], making it ideal for multilayer photonic device applications. In order to create highly sensitive devices, however, a meticulous study of its anisotropic dielectric properties is required. Furthermore, there has been considerable debate about the nature of ReS_2s band gap, with the recent consensus being that it is marginally indirect except in bilayer form [6,8,12,21,22]. Experimental studies that can shed light into this matter are essential.

In this work, we focus on high-resolution, polarization-resolved reflectance and PL at low temperature, discovering two additional exciton peaks that were predicted for ReS_2 [4] but not observed in previous studies. It is envisaged that these two shoulder peaks denoted by X_3 and X_4 are observed due to the splitting of spin degenerate excitonic states by combined effect of electron-hole exchange interaction, structural anisotropy, and spin-orbit coupling. X_3 and X_4 appear on the higher energy sides in both the absorption and PL measurements with similar polarization orientation as X_1 and X_2, respectively. The anisotropic nature of ReS_2s dielectric properties is further demonstrated via polarization-dependent reflectance. Transfer matrix method was utilized to understand the asymmetric excitonic lineshape in our reflectance from the $ReS_2/SiO_2/Si$ dielectric stack as a function of layer thickness and thus extract the real and imaginary part of anisotropic refractive index of the material. In addition, we report excitation polarization dependence of the PL, which provides insight into the anisotropic absorption of this material. For excitation energy 1.88 eV, the integrated PL intensity from all four exciton species is maximized when excitation polarization is oriented along X_2. Furthermore, our temperature-dependent study finds the four exciton peak positions are well resolved up to a temperature of 150 K, and their dipole orientations are preserved. Most intriguingly, we observe an anomalous PL intensity variation around 30 K, which necessitated the development of a model using rate equations, considering phonon scattering from low-lying dark exciton states. Our model provides evidence of the existence of indirect exciton states which are closely lying below the bright excitons, confirming the quasi-indirect nature of ReS_2s band gap. Our analysis can shed light on the understanding of the excitonic properties in this anisotropic material and provide useful information for photonics and optoelectronic device engineering with ReS_2.

Results and discussion. A schematic top view is shown in Fig. 1(a) of a single layer of ReS_2, where each molecular

*sajaldhara@phy.iitkgp.ac.in

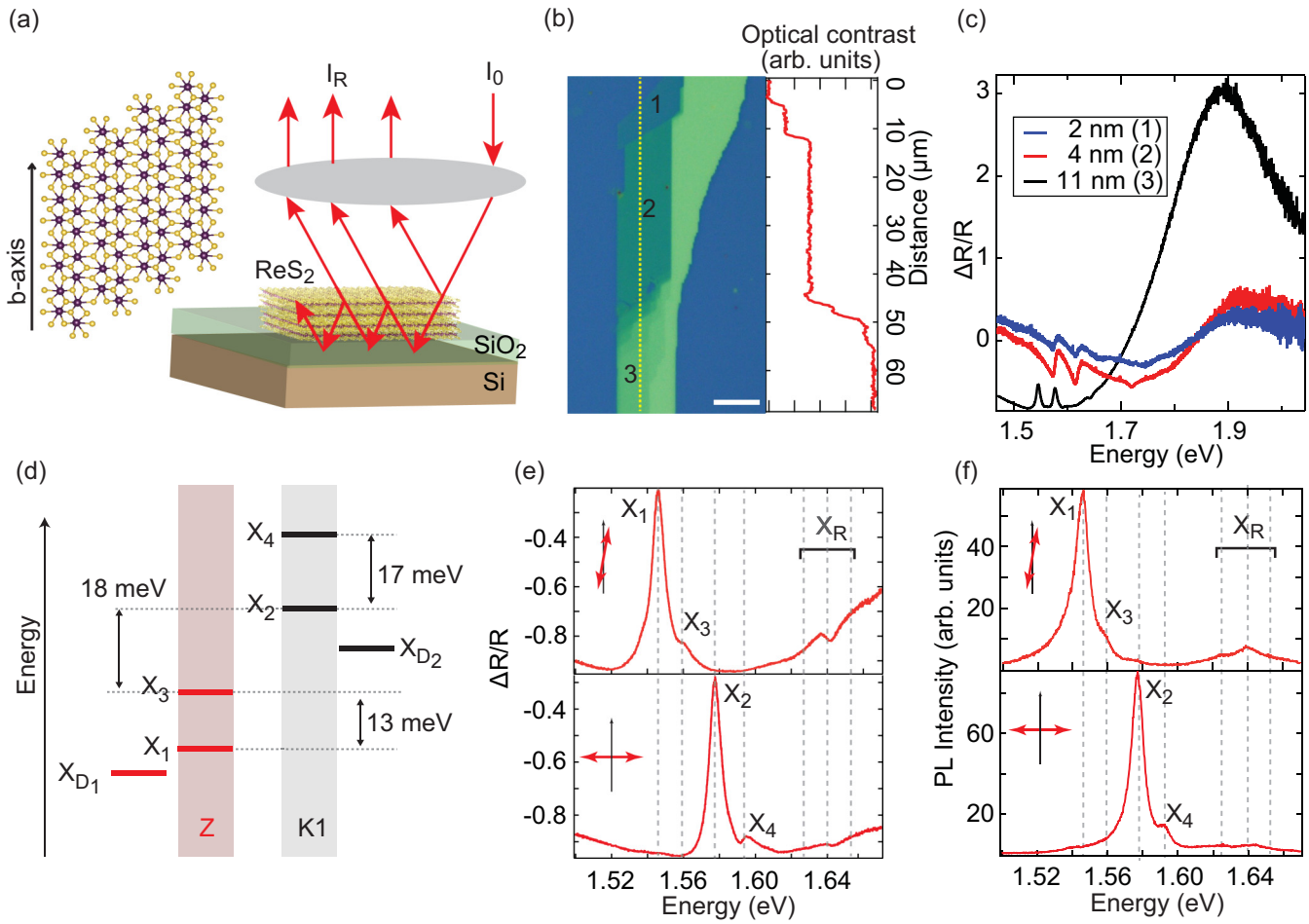

FIG. 1. (a) Top and side views of the distorted 1T phase of monolayer ReS_2. The arrow indicates the *b* axis of crystal orientation. (b) Optical microscope image of exfoliated ReS_2 transferred on Si/SiO_2 substrate. The white scale bar represents 10 μm. (left). Optical contrast along the dotted yellow line showing layer thickness (right). (c) Differential reflectance from unpolarized reflectance study at 3 different points in the sample marked as 1, 2, and 3 (2, 4, and 11 nm) in (b). Further studies are conducted on point 3, i.e., 11 nm ReS_2. (d) Schematic showing the exciton complexes at *Z* and *K*1 points of the Brillouin zone along with the low-lying momentum-dark states (e) Differential reflectance for two different incident polarizations with respect to the *b* axis as indicated in the inset of the top and bottom panel, showing four exciton peaks for 11 nm ReS_2. (f) Polarized PL intensity measured at two different orientations of the analyzer with respect to the *b* axis as indicated in the inset of the top and bottom panel. (e) and (f) corresponds to the polarization state for which the contribution is minimized from X_2 and X_4 (top) and X_1 and X_3 (bottom), respectively. X_R denotes the Rydberg excitations of X_1 and X_2.

layer is a sandwich of a Re layer between two S layers. The direction of the *b* axis is marked by a solid arrow which can be identified from the optical image during measurement. Sample was prepared by mechanical exfoliation technique, and dry transferred on to 340-nm SiO_2/Si substrate. The optical image of the sample is shown in Fig. 1(b) where we can approximately identify the number of layers from the optical contrast along a line profile, which has been further verified using AFM (see Fig. S1 in Ref. [23]). On-chip crystallographic orientation can be estimated by observing the sample edges, utilizing the fact that ReS_2 is likely to cleave along the axis containing the covalent Re-S bonds, which is parallel to the *b* axis [1,24].

Reflectance measurement was performed using a broadband halogen source with a spot size of $\sim 3\,\mu$m at three different points of the sample as shown in Fig. 1(b): points 1, 2, and 3, being 2, 4, and 11 nm thick, respectively. At 11-nm thickness (point 3), ReS_2 approaches its bulk character, wherein PL intensity becomes independent of the number of layers [1,2]. However, its 2D character is preserved since excitons are confined mostly in single layers [3].

Excitonic features in PL and reflectivity are too broad at room temperature to resolve all the peaks, therefore, the sample was cooled down to 3.2 K in a closed cycle cryostat. The reflectivity measured at points 1 and 2 show an asymmetric line shape about the excitonic resonance, as shown in Fig. 1(c). We see a pronounced red shift of exciton peak positions from few layers to bulk limit in agreement with previous reports [1,5,6]. In reflectivity data, we plot the differential reflectance, that is, $\frac{\Delta R}{R} = (R_{ReS_2+SiO_2/Si} - R_{SiO2/Si})/R_{SiO2/Si}$, where $R_{ReS_2+SiO_2/Si}$ and $R_{SiO_2/Si}$ are the reflectance spectra from the sample and the SiO_2/Si substrate, respectively. Due to interference in the multilayer film system consisting of Si, SiO_2 and ReS_2 as shown in the schematic in Fig. 1(a), a broad

anti-reflection dip coincides with the excitonic resonances. This makes the 11-nm ReS_2 (at point 3) ideal to probe well-resolved exciton peaks in reflectance, which almost mimics the PL spectrum. Chosen thickness of the SiO_2 layer and the dielectric properties of 11 nm ReS_2 make these peaks show a background free, almost symmetric Fano line shape. In contrast, the reflectivity measured at points 1 and 2 show asymmetric Fano line shape, which is a result of interference with the background reflectivity with a relative phase change of π across the exciton resonance [25]. The Fano asymmetry parameter varies across the three points. The peaks at higher energy range are the higher-order Rydberg series of the excitons [1,5]. What follows below are based on experimental results conducted on the 11-nm ReS_2.

We observe four peaks at 1.545 ± 0.001 (X_1), 1.558 ± 0.001 (X_3), 1.576 ± 0.001 (X_2), and 1.593 ± 0.001 (X_4) eV. The peaks at higher energy range are the higher-order Rydberg series of the excitons, denoted by X_2 [1,5]. The newly observed peaks X_3 and X_4 are in contrast to what has been observed earlier in $ReSe_2$ [3], since they appear at the higher energy side of X_1 and X_2, respectively. However, from the resemblance between these additional peaks and the similar peaks for $ReSe_2$, we speculate their origin is the splitting of singlet and triplet states of excitons due to electron-hole exchange interaction. Other plausible contributions for such splitting are the broken rotational symmetry due to structural anisotropy and spin-orbit coupling in ReS_2. As shown in Fig. 1(d), we attribute the higher energy prominent exciton transition X_2 to the $K1$ point, and X_1 to the Z point of the Brillouin zone, using the results of a recent, comprehensive *ab initio* calculation [8]. X_{D1} and X_{D2} are low-lying momentum-dark states nearly degenerate with X_1 and X_2, respectively. They will be of interest when considering temperature dependence of PL intensity later in this Rapid Communication. Figures 1(e) and 1(f) show the polarization resolved differential reflectance and PL at a polarization angle of -10° (top panels) and 90° (bottom panels), respectively, where all exciton peaks as seen in the reflectivity are also observed in PL with same energy positions. The 2-meV Stokes shift between PL emission and absorption peak (Fig. S2 in Ref. [23]) and the strong PL intensity indicates the pristine quality of our sample. We see no change in its optical properties over time and over multiple cooling cycles (Fig. S3 [23]).

In the polarization resolved reflectance measurement, linearly polarized white light was used as the source and the reflected light was collected via 0.7 NA objective lens, while the excitation polarization angle θ_P is varied with respect to the b axis using a half-wave plate. The experimental result for 11-nm ReS_2 is shown in the color plot in Fig. 2(a). A line plot in the bottom panel is chosen at an angle where we see all the four exciton resonances. The polar plot Fig. 2(b) shows that the two exciton species X_1 and X_2 are polarized at angles of 6° and 79° respectively with respect to the b axis (For fitting function see Ref. [23]), which agrees with earlier reported values within experimental error [1,8,26]. X_3 and X_4 follow the polarization variation of X_1 and X_2, respectively.

As shown in Fig. 1(a), we model the polarization resolved reflectance via transfer matrix technique [27–31] (see Ref. [23]) to obtain the reflectance spectrum of the $ReS_2/SiO_2/Si$ stack and hence extract the frequency-dependent dielectric function of ReS_2. We fit the polarization-resolved reflectance to obtain the dielectric function $\epsilon(\omega)$ for every polarization. The dielectric function is given by $\epsilon(\omega) = \epsilon_b + \sum \frac{f_i}{\omega_{0i}^2 - \omega^2 - i\omega\gamma_i}$, where ϵ_b, f_i, ω_{0i} and γ_i are the background dielectric constant, oscillator strength, resonance frequency and the linewidth of the i th oscillator, and the summation is over all exciton resonances. Figure 2(c) shows absolute reflectance spectra obtained at three different polarization angles of the linearly polarized incident beam, along with their theoretical fits. All the fitted parameters are given in Tables S1–S4 in Ref. [23].

The anisotropic refractive index $\tilde{n}(\hbar\omega) = n(\hbar\omega) + ik(\hbar\omega)$, where, n and k are the real and imaginary parts of refractive index, are shown in the color plots in Figs. 2(d) and 2(e), respectively. Interestingly, as shown in Fig. 2(c), we observed that the transfer matrix model best fit our experimental data with the polarization resolved reflectance only. However, Fig. S4 in Ref. [23], we show that it is not possible to obtain a good fit for unpolarized reflectance data with this model. As the unpolarized reflectance is a result of averaging over all polarization, it cannot be fitted by an effective value of the dielectric constant, since it is in truth highly anisotropic.

A 660-nm laser with a spot size of $\sim 1\ \mu$m is used to excite the sample with variable polarization with respect to the b axis. At first, the integrated PL was collected directly at the spectrometer slit without any analyzer at the output port. We discover that the overall PL intensity varies with the excitation polarization direction as shown in the color plot in Fig. 3(a). The intensity of the overall spectrum is modulated; however, the intensity ratio of X_1 and X_2 remains unchanged as the incident polarization is varied. Intensity from all exciton species is maximum at a particular polarization of excitation laser, corresponding to an in-plane direction which turns out to be the polarization direction of the X_2 exciton, within experimental error. This is a consequence of absorption at excitation energy 1.88 eV also being anisotropic, peaking at the angle along X_2. This can be predicted from the angle-dependent absorption obtained from our fitting (Fig. S5 [23]), and agrees with theoretical calculations [4]. The incident polarization dependence for two other lower excitation energies (1.76 and 1.70 eV) closer to X_2 resonance was also tested, which showed slightly different behavior (Fig. S6 [23]). The anisotropy becomes more pronounced as the excitation energy comes closer to the exciton resonances.

Next, we keep the excitation polarization fixed at an angle for which the overall PL is maximum and measure the polarization state of the PL via an analyzer placed before the spectrometer slit. Data shown in Fig. 3(b) were recorded while rotating the analyzer angle θ_A from 0° to 360°, where zero is along the b axis. From the polar plot in Fig. 3(d), we find the two dominant emission peaks at X_1 and X_2 are polarized with respect to the b axis at angles of 6° and 82°, respectively, which is same as the angles obtained from reflectance considering experimental error. It is observed as shown in Figs. 2(b) and 3(d) that the two shoulder peaks at X_3 and X_4 follow the same polarization directions as X_1 and X_2, respectively.

We perform a temperature-dependent PL measurement, the results of which are plotted in Fig. 4(a). The analyzer is fixed

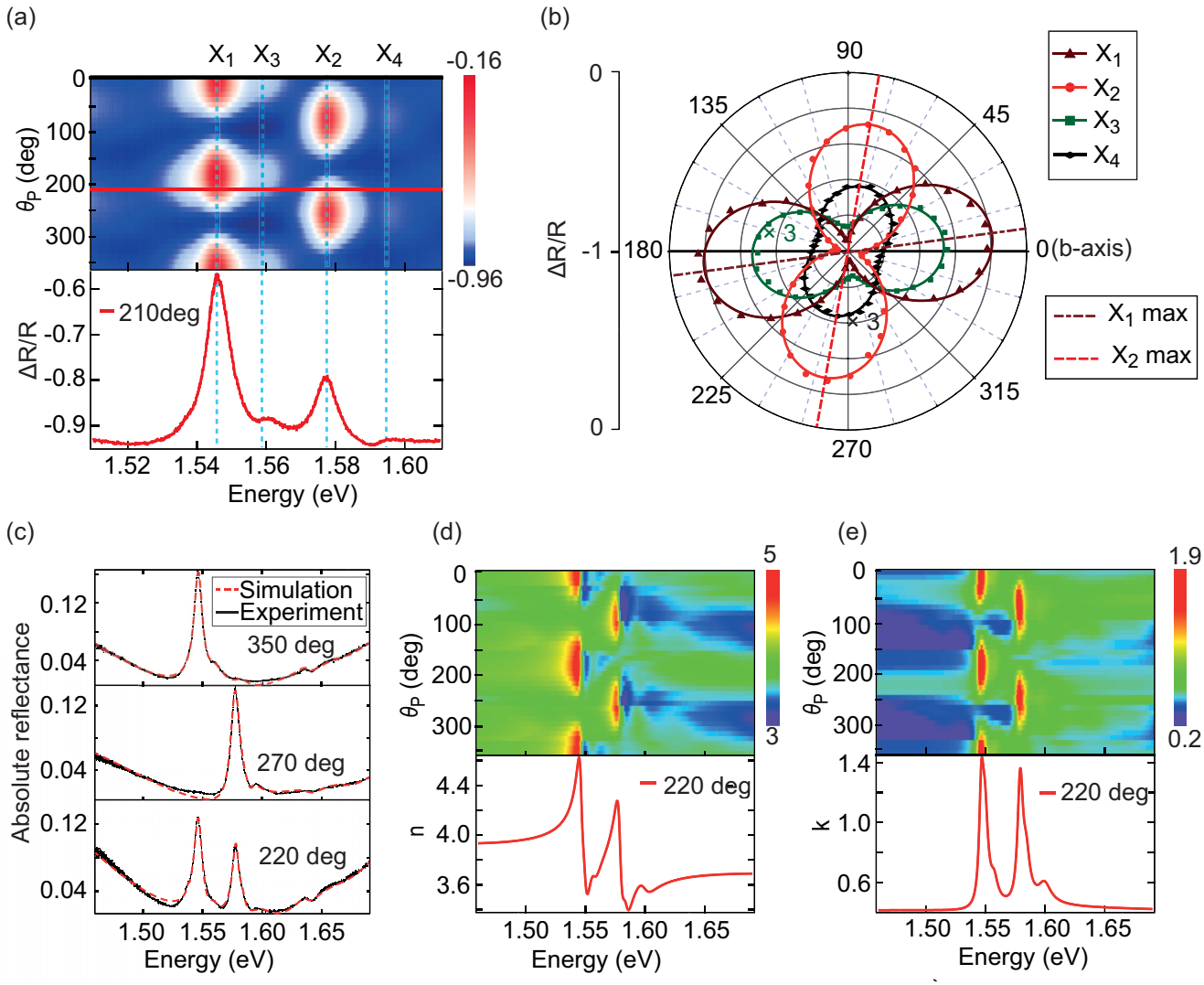

FIG. 2. (a) Color plot representing the differential reflectance spectrum as a function of incident polarization angle θ_P measured with respect to the *b* axis for 11 nm ReS_2. Line profile in the lower panel shows reflectance at a particular polarization angle where all four excitons can be observed. (b) Polar plots of differential reflectance for four different excitons X_1, X_2, X_3, and X_4 proportional to the oscillator strength (values for X_3 and X_4 are multiplied by 3 for clarity). (c) Polarization resolved absolute reflectance data (black) along with the simulation result (red) obtained from the transfer matrix method, shown for three different polarization angles. [(d) and (e)] Color plots demonstrating the in-plane anisotropy in the real and imaginary part of the refractive index, obtained from the fitting of absolute reflectance at variable polarization. The lower panel shows the corresponding line profile obtained at particular angle of polarization.

throughout at an angle for which all four exciton peaks are visible. The two shoulder peaks X_3 and X_4 are not resolvable above 150 K since they are dominated by X_1 and X_2 whose linewidths increase with temperature. We observe an anomalous temperature variation of PL intensity as shown in Fig. 4(c), with a maxima in intensity near 30 K, which can be attributed to the presence of low-lying dark states (X_{D1}, X_{D2}). Spin-forbidden dark excitons [32] have recently been reported to be the cause of anomalous temperature-dependent PL in group VI TMDCs [33]. On the other hand, momentum-forbidden low-lying states have been hypothesized before to explain the ratio of X_1 and X_2 populations not following the expected Boltzmann distribution [1,6]. This is also evident in Fig. 3 where it is observed that the X_1 PL intensity is lower than X_2 which is persistent even at higher temperatures as shown in Fig. 4(c). Time-resolved measurements have also revealed that the radiative lifetimes of excitons to be less than 10 ps [12], indicating the excitons are not thermalized.

To gain a comprehensive understanding of the temperature variation of this hot photoluminescence, we propose a rate equation model involving the bright (X_1, X_2) and dark states (X_{D1}, X_{D2}) as shown in the schematic diagram Fig. 4(b), where excitons in these states are generated via continuous wave (CW) pumping. Two kinds of phonon scattering are important in this model which are discussed below. First, scattering of excitons from X_{D1} to X_1 and X_{D2} to X_2 with rates γ_1 and γ_2 respectively, where E_{01} and E_{02} are the energy of the phonons involved. Second, α_1, α_2 and β_1, β_2 are the scattering rates from X_1 and X_2 to momentum-forbidden dark states outside the light cone. Excitons scatter to a continuum of states outside the light cone via phonons of all available energies. To simplify the model, we have considered only two different

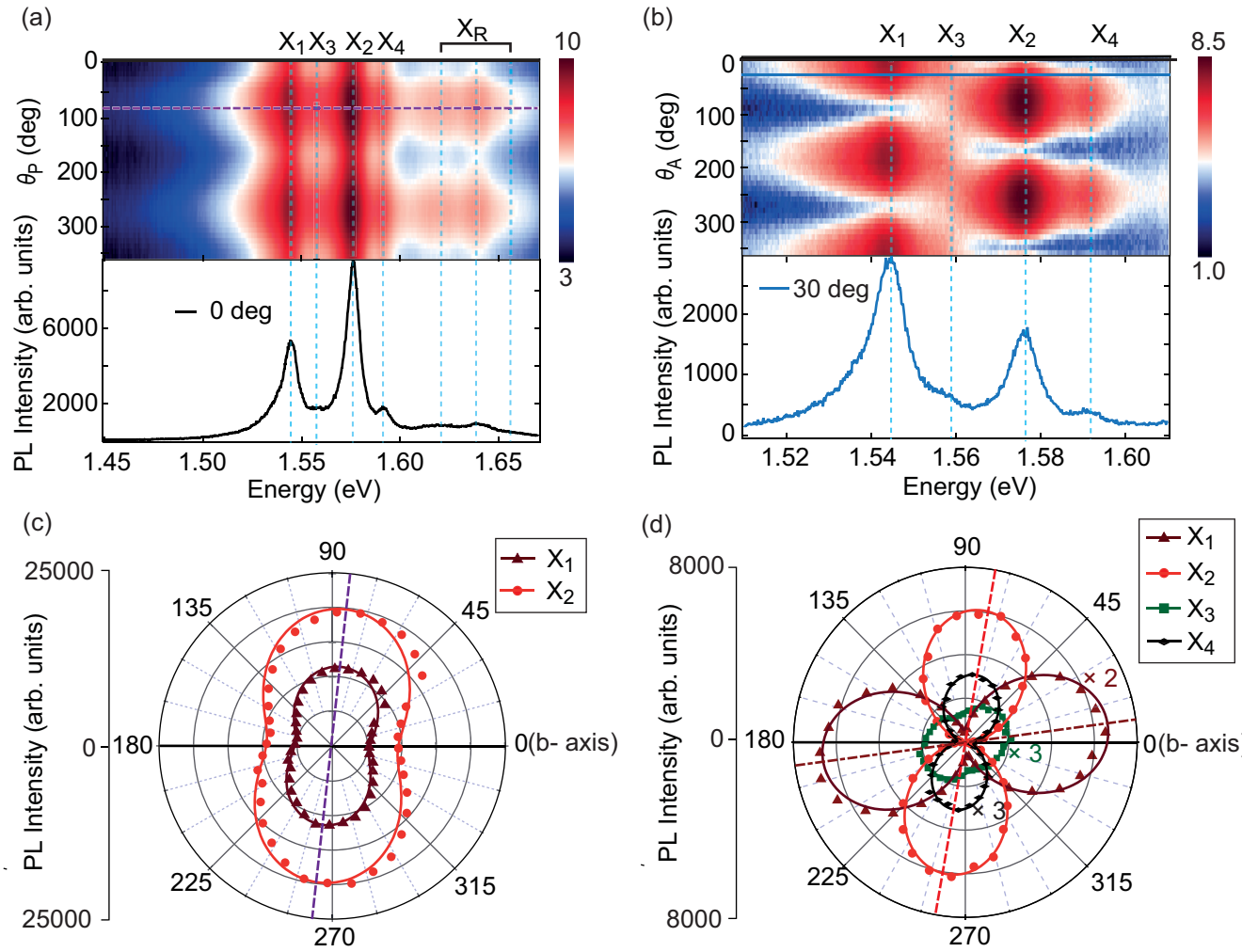

FIG. 3. (a) Color plot showing the PL spectrum in the log scale as a function of excitation laser polarization angle θ_P with respect to the b axis for 11-nm ReS_2 when no analyzer is placed at the output path. The dotted line indicates the polarization angle at which the overall PL intensity is maximum. The linear scale PL spectrum when the excitation laser aligned with the b axis is shown in the lower panel. (b) Color plot showing the PL spectrum in the logarithmic scale as a function of angle of the analyzer (with respect to b axis) obtained at a fixed polarization of the excitation laser which maximize the PL intensity. For the same excitation polarization, a linear scale PL spectrum at 30° angle of the analyser is shown in the lower panel. (c) Polar plot representing the PL intensity variation for two most prominent peaks, X_1 and X_2 as a function of the excitation polarization angle. (d) Polar plot representing the PL intensity variation of X_1, X_2, X_3, and X_4 as a function of the angle of the analyzer θ_P at fixed excitation polarization (Intensity of X_1, X_3 and X_4 are multiplied by factors of 2, 3, and 3 respectively for clarity). The dotted lines indicate corresponding angle of maximum PL for X_1 and X_2 excitons.

phonon energies per exciton state: E_{1n}, E_{1m} for X_1 and E_{2n}, E_{2m} for X_2. This effectively accounts for the scattering at both low temperature and high temperature regimes (see Fig. S10 in Ref. [23]).

We assume τ_1 and τ_2 are the radiative recombination times from X_1 and X_2, and τ_{D1} and τ_{D2} are the nonradiative recombination times from X_{D1} and X_{D2}. By solving the rate equation under CW excitation (see Ref. [23]), the PL intensity for X_1 and X_2 is obtained as a function of temperature, and fitted with the experimental data as shown in Fig. 4(c). From this model we find the two momentum-dark states X_{D1} and X_{D2} are present 16 and 5 meV below X_1 and X_2 states, respectively. These dark states strongly indicate a quasi-indirect band gap at Z and $K1$ points in the Brillouin zone. This is in agreement with *ab initio* calculations which indicate ReS_2 is marginally indirect [6,8].

When temperature is initially increased (3.2 K $< T <$ 30 K) X_1 and X_2 are thermally populated from X_{D1} and X_{D2} states by absorbing phonons. At the same time, X_1 and X_2 excitons are scattered from the radiative window to outside the light cone, where they recombine nonradiatively, by absorbing phonons of energy 17 and 3.2 meV, respectively. In this temperature regime, we observe dark states are appreciably more populated than bright states on laser excitation, which results in a net gain in excitons scattered to the bright states. This causes PL intensity to increase to a maximum at 30 K. At higher temperatures, the scattering process is mainly dominated by phonons of energies 52 and

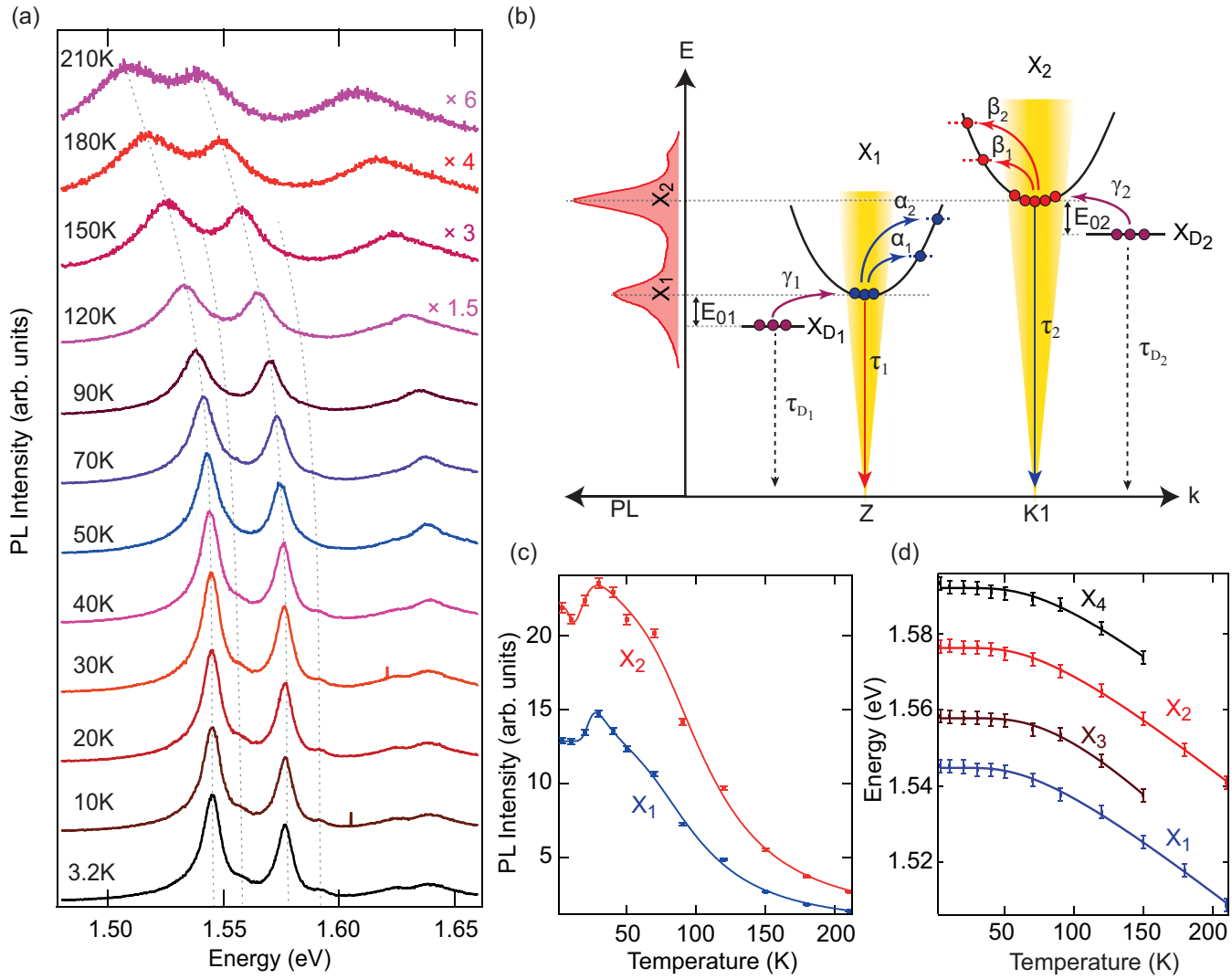

FIG. 4. (a) PL spectra measured at different temperatures for a fixed angle of the analyser and excitation polarization. The dotted lines are a guide to eye. (b) Schematic diagram for the rate equation model. Curved arrows indicate all the phonon scattering processes considered in the model. Black dotted lines indicate nonradiative decay channel. Yellow region indicates the light cone for momentum allowed optical transitions. The solid straight arrows represent radiative decay channels. (c) Variation of PL intensity with temperature showing a local maxima around 30 K. Blue and red solid lines are fits obtained from the rate equation model. (d) Peak positions for the four excitons as a function of temperature. Solid lines are the fitted curves from the theoretical model.

41 meV from X_1 and X_2 states respectively. Scattering to dark states increases more rapidly than that to bright states after 30 K, causing PL intensity to decrease. All phonon energies obtained, except for 5 and 3.2 meV, have recently been reported for ReS_2 [34]. From our fitting we also notice that the effective scattering time from X_1 and X_2 is much more than their recombination times, even up to high temperatures, which corroborates the fact that X_1 and X_2 emit hot photoluminescence.

We plot the observed redshift of exciton peak positions with temperature, and fit with the model describing the temperature dependence of a semiconductor band gap [35]: $E_g(T) = E_g(0) - S\hbar\omega[\coth(\frac{\hbar\omega}{2kT}) - 1]$. Here, $E_g(0)$ is the exciton resonance energy at T = 0 K, S is a dimensionless electron-phonon coupling constant, and $\hbar\omega$ is the average phonon energy. The fitted parameters are $E_g(0)$, S and $\hbar\omega$. The values of S are 1.74, 1.78, 2.42, and 1.83 for X_1, X_2, X_3, and X_4, respectively, and $\hbar\omega$ is around 20 ± 3 meV, concurring with earlier reports [36,37]. Energy separation between the four exciton peaks remains constant with temperature as can be seen in Fig. 4(d). The angle between the excitons dipole moment orientation and b axis remains unchanged with temperature indicates the temperature independent anisotropy (Fig. S7 [23]). Finally, temperature-dependent reflectance measurements were used to acquire the corresponding dielectric function using the transfer matrix method (Fig. S8 [23]). ϵ_1 shows significant change only near the exciton resonances.

Conclusion. In conclusion, we observed two additional exciton shoulder peaks at higher energy sides of X_1 and X_2 which are attributed to splitting of spin degenerate exciton states. The *ab initio* calculations required to systematically

investigate the exact origin of this splitting is beyond the scope of this work, and may be carried out in future studies. The transfer matrix method is utilized to extract the in-plane anisotropic complex dielectric function of several-layer ReS_2 in unprecedented detail, which is crucial for modeling photonic devices or further experiments that make use of its anisotropic optical properties. Our temperature-dependent study reveals an anomalous temperature variation in the PL intensity which underpins the existence of low-lying dark states, indicating quasi-indirect band gap in this system. The proposed mechanism considering the dynamical processes not only explains the observed temperature variation but also estimates the phonon energies supported by previous reports. It also establishes temperature-dependent study as an accessible method to probe the existence of low-lying optically dark states.

Acknowledgments. We acknowledge D. K. Goswami and his group for the Atomic Force Microscope measurement on the sample. S. D. acknowledges Science and Engineering Research Board (SB/S2/RJN-110/2016) Ramanujan Fellowship, Indian Institute of Technology Kharagpur (IIT/SRIC/ISIRD/2017-2018), and Ministry of Human Resource Development (IIT/SRIC/PHY/NTS/2017-18/75) for the funding and support for this work. D. C. acknowledges Council of Scientific and Industrial Research , JRF (09/081(1352)/2019-EMR-I) for the financial assistance. We thank C. Chakraborty, A. Arora, and P. K. Chakraborty for their valuable comments on this work.

[1] O. B. Aslan, D. A. Chenet, A. M. van der Zande, J. C. Hone, and T. F. Heinz, Linearly polarized excitons in single- and few-layer ReS_2 crystals, ACS Photonics **3**, 96 (2016).

[2] S. Tongay, H. Sahin, C. Ko, A. Luce, W. Fan, K. Liu, J. Zhou, Y.-S. Huang, C.-H. Ho, J. Yan, D. F. Ogletree, S. Aloni, J. Ji, S. Li, J. Li, F. M. Peeters, and J. Wu, Monolayer behavior in bulk ReS_2 due to electronic and vibrational decoupling, Nat. Commun. **5**, 3252 (2014).

[3] A. Arora, J. Noky, M. Drüppel, B. Jariwala, T. Deilmann, R. Schneider, R. Schmidt, O. Del Pozo-Zamudio, T. Stiehm, A. Bhattacharya, P. Krüger, S. Michaelis de Vasconcellos, M. Rohlfing, and R. Bratschitsch, Highly anisotropic in-plane excitons in atomically thin and bulklike 1 T'-ReSe $_2$, Nano Lett. **17**, 3202 (2017).

[4] J. P. Echeverry and I. C. Gerber, Theoretical investigations of the anisotropic optical properties of distorted 1 T ReS_2 and $ReSe_2$ monolayers, bilayers, and in the bulk limit, Phys. Rev. B **97**, 075123 (2018).

[5] J. Jadczak, J. Kutrowska-Girzycka, T. Smoleński, P. Kossacki, Y. S. Huang, and L. Bryja, Exciton binding energy and hydrogenic Rydberg series in layered ReS_2, Sci. Rep. **9**, 1578 (2019).

[6] J. M. Urban, M. Baranowski, A. Kuc, Ł. Kłopotowski, A. Surrente, Y. Ma, D. Włodarczyk, A. Suchocki, D. Ovchinnikov, T. Heine, D. K. Maude, A. Kis, and P. Plochocka, Non equilibrium anisotropic excitons in atomically thin ReS_2, 2D Mater. **6**, 015012 (2018).

[7] S. Sim, D. Lee, A. V. Trifonov, T. Kim, S. Cha, J. H. Sung, S. Cho, W. Shim, M.-H. Jo, and H. Choi, Ultrafast quantum beats of anisotropic excitons in atomically thin ReS_2, Nat. Commun. **9**, 351 (2018).

[8] R. Oliva, M. Laurien, F. Dybala, J. Kopaczek, Y. Qin, S. Tongay, O. Rubel, and R. Kudrawiec, Pressure dependence of direct optical transitions in ReS_2 and $ReSe_2$, npj 2D Mater Appl **3**, 20 (2019).

[9] E. Liu, Y. Fu, Y. Wang, Y. Feng, H. Liu, X. Wan, W. Zhou, B. Wang, L. Shao, C.-H. Ho, Y.-S. Huang, Z. Cao, L. Wang, A. Li, J. Zeng, F. Song, X. Wang, Y. Shi, H. Yuan, H. Y. Hwang, Y. Cui, F. Miao, and D. Xing, Integrated digital inverters based on two-dimensional anisotropic ReS_2 field-effect transistors, Nat. Commun. **6**, 6991 (2015).

[10] Q. Cui, J. He, M. Z. Bellus, M. Mirzokarimov, T. Hofmann, H.-Y. Chiu, M. Antonik, D. He, Y. Wang, and H. Zhao, Transient absorption measurements on anisotropic monolayer ReS_2, Small **11**, 5565 (2015).

[11] Y. Zhou, N. Maity, A. Rai, R. Juneja, X. Meng, A. Roy, Y. Zhang, X. Xu, J.-F. Lin, S. K. Banerjee, A. K. Singh, and Y. Wang, Stacking-order-driven optical properties and carrier dynamics in ReS_2, Adv. Mater. **32**, 1908311 (2020).

[12] X. Wang, K. Shinokita, H. E. Lim, N. B. Mohamed, Y. Miyauchi, N. T. Cuong, S. Okada, and K. Matsuda, Direct and indirect exciton dynamics in few-layered ReS_2 revealed by photoluminescence and pump-probe spectroscopy, Adv. Funct. Mater. **29**, 1806169 (2019).

[13] S. Sim, D. Lee, M. Noh, S. Cha, C. H. Soh, J. H. Sung, M.-H. Jo, and H. Choi, Selectively tunable optical Stark effect of anisotropic excitons in atomically thin ReS_2, Nat. Commun. **7**, 13569 (2016).

[14] M. Hafeez, L. Gan, A. Saleem Bhatti, and T. Zhai, Rhenium dichalcogenides (ReX_2, X = S or Se): An emerging class of TMDs family, Mater. Chem. Front. **1**, 1917 (2017).

[15] J. Wilson and A. Yoffe, The transition metal dichalcogenides discussion and interpretation of the observed optical, electrical and structural properties, Adv. Phys. **18**, 193 (1969).

[16] S. Sim, D. Lee, J. Lee, H. Bae, M. Noh, S. Cha, M.-H. Jo, K. Lee, and H. Choi, Light polarization-controlled conversion of ultrafast coherent–incoherent exciton dynamics in few-layer ReS_2, Nano Lett. **19**, 7464 (2019).

[17] J. Wang, Y. J. Zhou, D. Xiang, S. J. Ng, K. Watanabe, T. Taniguchi, and G. Eda, Polarized light-emitting diodes based on anisotropic excitons in few-layer ReS_2, Adv. Mater. **32**, 2001890 (2020).

[18] E. Zhang, Y. Jin, X. Yuan, W. Wang, C. Zhang, L. Tang, S. Liu, P. Zhou, W. Hu, and F. Xiu, ReS_2-based field-effect transistors and photodetectors, Adv. Funct. Mater. **25**, 4076 (2015).

[19] J. Kwon, Y. Shin, H. Kwon, J. Y. Lee, H. Park, K. Watanabe, T. Taniguchi, J. Kim, C.-H. Lee, S. Im, and G.-H. Lee, All-2D ReS_2 transistors with split gates for logic circuitry, Sci. Rep. **9**, 10354 (2019).

[20] A. Splendiani, L. Sun, Y. Zhang, T. Li, J. Kim, C.-Y. Chim, G. Galli, and F. Wang, Emerging photoluminescence in monolayer MoS_2, Nano Lett. **10**, 1271 (2010).

[21] D. Biswas, A. M. Ganose, R. Yano, J. M. Riley, L. Bawden, O. J. Clark, J. Feng, L. Collins-Mcintyre, M. T. Sajjad, W. Meevasana, T. K. Kim, M. Hoesch, J. E. Rault, T. Sasagawa,

D. O. Scanlon, and P. D. C. King, Narrow-band anisotropic electronic structure of ReS_2, Phys. Rev. B **96**, 085205 (2017).

[22] J. L. Webb, L. S. Hart, D. Wolverson, C. Chen, J. Avila, and M. C. Asensio, Electronic band structure of ReS_2 by high-resolution angle-resolved photoemission spectroscopy, Phys. Rev. B **96**, 115205 (2017).

[23] See Supplemental Material at http://link.aps.org/supplemental/10.1103/PhysRevB.102.161404 for additional data and modeling.

[24] C. Liang, Y. Chan, K. Tiong, Y. Huang, Y. Chen, D. Dumcenco, and C. Ho, Optical anisotropy of Au-doped ReS_2 crystals, J. Alloys Compd. **480**, 94 (2009).

[25] M. F. Limonov, M. V. Rybin, A. N. Poddubny, and Y. S. Kivshar, Fano resonances in photonics, Nat. Photonics **11**, 543 (2017).

[26] C.-H. Ho and Z.-Z. Liu, Complete-series excitonic dipole emissions in few layer ReS_2 and $ReSe_2$ observed by polarized photoluminescence spectroscopy, Nano Energy **56**, 641 (2019).

[27] P. Blake, E. W. Hill, A. H. Castro Neto, K. S. Novoselov, D. Jiang, R. Yang, T. J. Booth, and A. K. Geim, Making graphene visible, Appl. Phys. Lett. **91**, 063124 (2007).

[28] Y. Li, A. Chernikov, X. Zhang, A. Rigosi, H. M. Hill, A. M. van der Zande, D. A. Chenet, E.-M. Shih, J. Hone, and T. F. Heinz, Measurement of the optical dielectric function of monolayer transition-metal dichalcogenides: $MoS1_2$, $MoSe_2$, WS_2, and WSe_2, Phys. Rev. B **90**, 205422 (2014).

[29] H. Zhang, Y. Ma, Y. Wan, X. Rong, Z. Xie, W. Wang, and L. Dai, Measuring the refractive index of highly crystalline monolayer MoS_2 with high confidence, Sci. Rep. **5**, 8440 (2015).

[30] C. Hsu, R. Frisenda, R. Schmidt, A. Arora, S. M. Vasconcellos, R. Bratschitsch, H. S. J. der Zant, and A. Castellanos-Gomez, Thickness-dependent refractive index of 1L, 2L, and 3L MoS_2, $MoSe_2$, WS_2, and WSe_2, Adv. Opt. Mater. **7**, 1900239 (2019).

[31] A. B. Kuzmenko, Kramers–Kronig constrained variational analysis of optical spectra, Rev. Sci. Instrum. **76**, 083108 (2005).

[32] M. R. Molas, C. Faugeras, A. O. Slobodeniuk, K. Nogajewski, M. Bartos, D. M. Basko, and M. Potemski, Brightening of dark excitons in monolayers of semiconducting transition metal dichalcogenides, 2D Mater. **4**, 021003 (2017).

[33] A. Arora, N. K. Wessling, T. Deilmann, T. Reichenauer, P. Steeger, P. Kossacki, M. Potemski, S. Michaelis de Vasconcellos, M. Rohlfing, and R. Bratschitsch, Dark trions govern the temperature-dependent optical absorption and emission of doped atomically thin semiconductors, Phys. Rev. B **101**, 241413(R) (2020).

[34] A. McCreary, J. R. Simpson, Y. Wang, D. Rhodes, K. Fujisawa, L. Balicas, M. Dubey, V. H. Crespi, M. Terrones, and A. R. Hight Walker, Intricate Resonant Raman Response in Anisotropic ReS_2, Nano Lett. **17**, 5897 (2017).

[35] K. P. O'Donnell and X. Chen, Temperature dependence of semiconductor band gaps, Appl. Phys. Lett. **58**, 2924 (1991).

[36] C. H. Ho, Y. S. Huang, K. K. Tiong, and P. C. Liao, Absorption-edge anisotropy in ReS_2 and $ReSe_2$ layered semiconductors, Phys. Rev. B **58**, 16130 (1998).

[37] C.-H. Ho, Optical study of the structural change in ReS_2 single crystals using polarized thermoreflectance spectroscopy, Opt. Express **13**, 8 (2005).